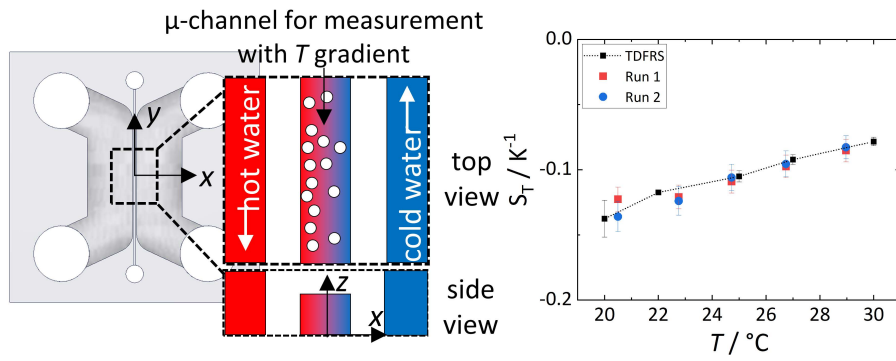


Graphical Abstract

Thermophoretic microfluidic cells for evaluating Soret coefficient of colloidal particles

Namkyu Lee, Shilpa Mohanakumar, Simone Wiegand



Highlights

Thermophoretic microfluidic cells for evaluating Soret coefficient of colloidal particles

Namkyu Lee, Shilpa Mohanakumar, Simone Wiegand

- We propose a thermophoretic microfluidic cell to measure the Soret coefficient quantitatively
- Verification of one-dimensional temperature and concentration gradient in cell
- We demonstrate that the obtained Soret coefficients agree with a validated method

Thermophoretic microfluidic cells for evaluating Soret coefficient of colloidal particles

Namkyu Lee^a, Shilpa Mohanakumar^a and Simone Wiegand^{a,b,*}

^aIBI-4, Forschungszentrum Jülich, 52428, Germany

^bUniversität zu Köln, 50939, Germany

ARTICLE INFO

Keywords:

Thermophoresis, Microfluidics, Temperature gradient, Soret coefficient, Colloidal particles

ABSTRACT

Thermodiffusion or thermophoresis gained much interest in bio, chemical, and energy engineering. Although there are several methods to measure thermophoresis, they consume large sample volumes, are limited to binary mixtures, and give only indirect access to the applied temperature profile. Herein, we propose a thermophoretic microfluidic cell for quantitative measurements of the Soret coefficient of colloids. The actual microscale measuring channel lies between cooling and heating channels to achieve a one-dimensional temperature gradient. Fluorescence lifetime imaging microscopy with Rhodamine B is utilized to measure the spatial temperature profile in the channel. The fluorescence intensity of fluorescently labeled polystyrene particles with a diameter of 25 nm is used to monitor the concentration profile. The observed temperature and concentration profiles are one-dimensional, as gradients in the longitudinal and height directions can be neglected. In the investigated temperature range, the averaged difference between the measured Soret coefficients with the cell and determined with the Thermal Diffusion Forced Rayleigh Scattering set-up is less than 8%.

1. Introduction

Thermodiffusion or thermophoresis is a process which occurs in non-isothermal systems, when a temperature gradient drives not only a heat flux, but also a mass flux [1]. This coupling of heat and mass fluxes leads to a concentration profile and plays a role in natural and technical transport processes with temperature gradients, e.g. petrology (rock formation), petroleum reservoirs and as separation techniques [2]. Also, as it is one of the few known mechanisms which allows the accumulation of substance against diffusion it is discussed in the context of the origin-of-life question [3, 4]. In the recent years, it has turned out that the thermophoretic response of proteins and protein-ligand complexes can be used to characterize the binding affinity between ligand and protein utilizing the so-called microscale thermophoresis device (MST) [5, 6, 7]. Furthermore, the effect also needs to be considered in the development of liquid thermoelectric cells used to convert waste heat into electricity [8, 9, 10]. In those cells, charged colloidal particles are added to increase the energy conversion efficiency. To improve our still poor understanding of physicochemical effect and to develop improved theoretical concepts of thermophoresis in those multicomponent systems, quantitative measurements are desirable [11].

Thermophoresis is the particle movement driven by a temperature gradient [6], which is expressed by the flux equation [12]

$$\vec{j} = -\rho D \nabla c - \rho c(1-c) D_T \nabla T \quad (1)$$


with the net mass flux j , the particle density ρ , the diffusion coefficient D , the concentration c of the solute, the thermal

diffusion coefficient D_T and the temperature T . In the steady state ($\vec{j} = 0$), the Soret coefficient, S_T , is defined as $S_T \equiv D_T/D$. The Soret coefficient S_T is a measure for the resulting concentration difference Δc , if a certain temperature difference ΔT is applied. Despite many theoretical approaches and simulations [2, 13, 14, 15, 16], there is so far no microscopic theory which predicts S_T quantitatively. While mass, shape and moment of inertia are important for thermodiffusive properties of non-polar substances, the thermodiffusion of polar and especially aqueous solutions is governed by the hydrophilicity of the solute molecules, pH and ionic strength [6].

There are several experimental methods to measure the Soret coefficient quantitatively, such as thermal lens (TL) [17, 18], Thermal Diffusion Forced Rayleigh Scattering (TDFRS) [19, 20], beam deflection [21, 22, 23] and thermogravitational columns (TCs) [24]. Except for TCs, all other methods use optical detection and depend on the optical refractive index contrast due to temperature and concentration changes. Therefore, they are limited to binary or specific ternary systems unless two wavelengths are implemented using the dispersion to analyze ternary systems [25]. For the multi-component mixtures, TC, which uses the interaction of free convection and thermodiffusive flow, is a good choice [24, 26] as samples are drawn from the column and analyzed according to their composition. However, TCs consume sample volumes in the order of 30 mL [24], which are not affordable for biological samples only available in small amounts of a few micro liter.

To overcome limitations of conventional measurement methods, advanced microfluidic devices have been suggested [27, 28, 29, 30]. In general, microfluidic devices consume small sample volumes ($\sim \mu\text{L}$) and provide short equilibrium times so that they are suitable for biological samples. An instrument utilizing the thermophoretic effect

*Corresponding author

 n.lee@fz-juelich.de (N. Lee); s.wiegand@fz-juelich.de (S. Wiegand)

Wiegand)

ORCID(s):

is MST [28] which has been widely used for investigating diseases such as influenza [31], corona[32] and Alzheimer [33]. While the strengths of MST are a low detection limit (~ 1 pM) and a fast response time to measure the protein-ligand binding constant, it gives only qualitative values for the Soret coefficient. Researchers have also used microfluidic channels to quantify the Soret coefficient [27, 29, 30]. The main difficulty of microfluidic cells is the reliable determination of the temperature and concentration profile. Some experiments measure the temperature outside the actual measuring channel and assume an one-dimensional temperature profile propagating into the measuring channel [27, 30]. Otherwise, the temperature dependence of the fluorescence intensity in the measuring channel is used [29, 34]. Both methods are prone to errors, since it can easily be affected by changes in external condition such as the surrounding temperature for the first method or by photobleaching of the dye or reflections in the latter method [35].

In order to obtain reliable thermophoretic results, several points need to be considered. As S_T is proportional to $\Delta c / \Delta T$, a large temperature gradient causes a larger and easier to measure concentration difference. On the other hand, larger gradients can induce free convection, which mixes the solution and decreases the concentration differences resulting in too small measured Soret coefficients. Ideally, the channel shape induces an one-dimensional temperature profile, but, due to the small dimensions, the linearity is easily affected by external thermal conditions through conduction and convection [36]. This requires a comprehensive thermal analysis of the device, and a direct measurement of temperature and concentration is required.

Herein, we suggest a thermophoretic microfluidic cell made of poly(methyl methacrylate) (PMMA). We designed large cooling and heating channels with high mass flow rates up to 0.94 m/s leading to high temperature gradients up to 34000 K/m corresponding to a temperature difference of 3°C across the measuring channel. A confocal microscope with a photomultiplier and a correlator is used to measure the fluorescent lifetime correlation function. The temperature dependence of the lifetime is used to characterize the temperature profile within the measuring channel. Additionally, in order to calculate the Soret coefficient, we determined the concentration profile by measuring the fluorescence intensity. Aqueous solutions of polystyrene particles containing a fluorescent dye (Firefly, green) in the core of the particle with a diameter of 25 nm (G25) are used for validating the cell compared to TDFRS.

2. Method and Materials

2.1. Geometry and fabrication

Figure 1 (a) and (b) show a schematic and a picture of the thermophoretic microfluidic cell. The cell is made of PMMA, a transparent, bio-compatible and hard polymer. The measuring channel has been micro-milled between a heating and cooling channel. The cell is sealed with a

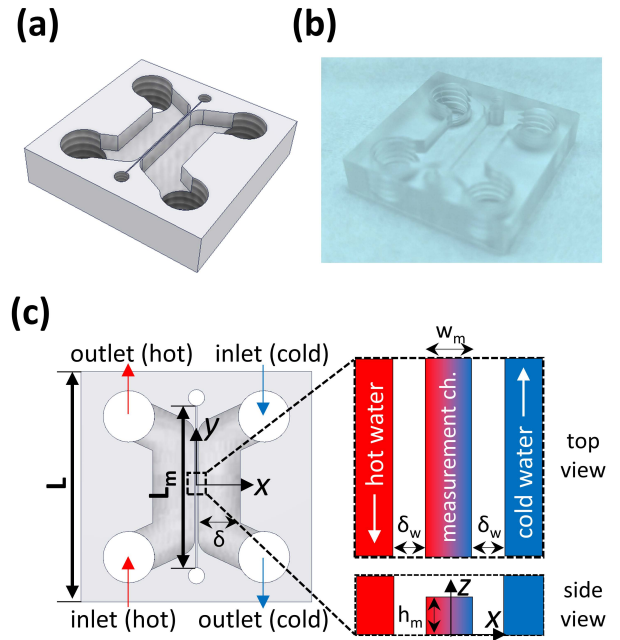


Figure 1: (a) Schematic drawing and (b) picture of the thermophoretic microfluidic cell. (c) Geometrical target dimensions of the cell are given in the text. Note, that the origin of the coordinate system is in the center of the measuring channel.

polyvinyl acetate (PVA) cover slip with a thickness of 170 μm . As an adhesive, we used a mixture of dichloromethane and cyclohexane with a volume ratio of 45 to 55.

Geometrical dimensions of the cell are presented in Fig. 1(c). The thickness of the PMMA block is 5 mm and its length is 22 mm to have sufficient space to attach connectors for the cooling and heating channels. The height and width (δ) of cooling and heating channels are 2.2 mm and 4.0 mm, respectively. We maximized the cross-section to reduce the pressure drop in the thermostating channels. The target width (w_m) and height (h_m) of the measuring channel are 127 μm and 100 μm , respectively. However, the fabrication process has a tolerance which is on the order of 20 μm [37] leading to slightly different dimensions which occur along the measuring channel. Using a fluorescent solution inside the measuring channel, we determined $w_m = 93.9$ μm and $h_m = 76$ μm for the fabricated cell. The length of the measuring channel (L_m) is 15 mm. The target wall thickness (δ_w) between the measuring channel and the cooling or heating channel is 100 μm . The ideal volume of the measuring channel is 0.2 μL .

2.2. Experimental set up

Figure 2 (a) and (b) present the experimental setup of the light and flow path to monitor the sample in the thermophoretic microfluidic cell, respectively. A confocal microscope (Olympus IX-71 with FV3-294 confocal unit) was used for observing the fluorescence intensity and lifetime. A pulsed laser with a wavelength of 485 nm was selected for excitation of the dye in combination with a long-pass emission filter at 500 nm (HQ 500 LP, Leica Microsystem

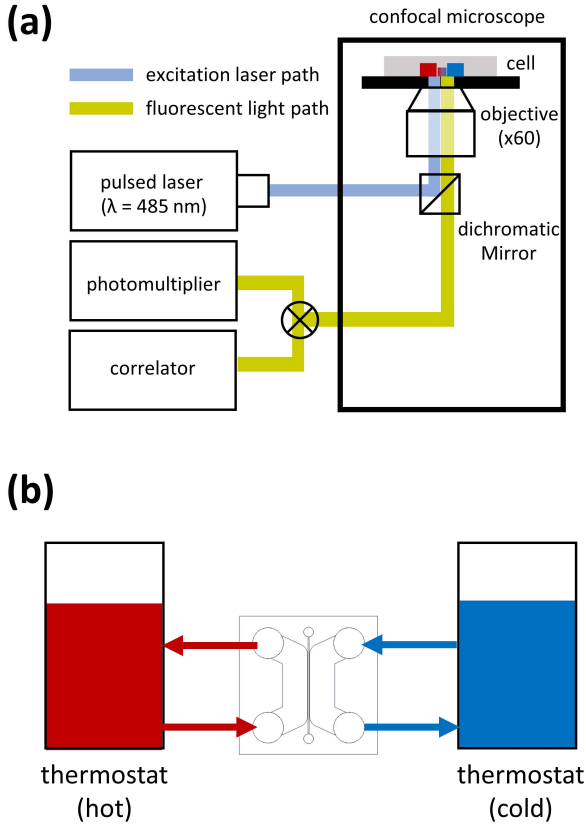


Figure 2: (a) Light path in the confocal microscope for measuring the Soret coefficient by using the thermophoretic microfluidic cell. (b) Microfluidic cell with cooling and heating channel to induce the temperature gradient.

GmbH, Wetzlar, Germany). The fluorescence intensity was recorded by a photomultiplier and the fluorescence lifetime was probed by fluorescence lifetime imaging microscopy (FLIM) using a correlator (PicoQuant, Berlin, Germany). In order to regulate the temperature in the cooling and heating channel, we used two thermostats (cooling: Lauda eco RE 620, Lauda-Königshofen, Germany, heating: Lauda ecoline RE 306, Lauda-Königshofen, Germany). To compensate the heat exchange between thermostating channels, we used a counter-flow to maintain a constant temperature gradient along the measuring channel. The controlled mass flow rate by thermostats was maximized to 520 ± 15 g/min. The low temperature was between 5°C and 15°C , and the high temperature was varied between 35°C and 45°C .

2.3. Sample preparation

We used polystyrene (PS) particles (G25, ThermoFisher Scientific Inc.) with a diameter of 25 nm without further treatment. The particles contained inside the core Firefly fluorescence green dye. At $T = 25^\circ\text{C}$ the particle density and the refractive index at a wavelength of 589 nm are $\rho = 1.05\text{g/cm}^3$ and $n = 1.59$, respectively. The particle concentration in a water-based solution with $\text{pH} = 3.2$ is 1 wt%. According to the supplier, ethylenediaminetetraacetic acid

(EDTA) and an anionic surfactant were added to stabilize the solution and to prevent aggregation[38].

Solutions are injected into the measuring channel through tubes and syringes by hand. The solutions are filtered through a $0.2\ \mu\text{m}$ filter (Whatman Anotop 10) which removes larger particles and the aggregation of the solutions. After that, the measuring channel is closed tightly by a lid to prevent evaporation and concentration changes during the measurement.

For measuring the solutions in TDFRS, the filtered solution is filled into an optical quartz cell (Hellma) with an optical path length 0.2 mm. Solutions were measured two times at the same temperature. Auxiliary parameters, concentration and temperature dependence of the refractive index, are required to calculate Soret coefficient S_T . The refractive index as function of concentration was measured with an Abbe refractometer (Anton Paar Abbemat MW) at a read-out wavelength of 632.8 nm. We measured the refractive index for 5 concentrations to determine $(\partial n / \partial c)_{p,T}$. The change of the refractive index with respect to temperature, $(\partial n / \partial T)_{p,c}$ was measured interferometrically [39].

2.4. Temperature and concentration ratio measurement

The averaged decaying time of the fluorescence intensity from an excited to ground state typically depends on temperature, therefore we use this temperature sensitivity of the fluorescence lifetime to measure the temperature inside the measuring channel [40]. As fluorescent dye, we used Rhodamine B (RhB, Sigma Aldrich, grade: for fluorescence). The fluorescent correlation function can be recorded for each position in the measuring channel and is then analyzed with a commercial software (SymPhoTime provided by PicoQuant). Using a calibration curve between fluorescence lifetime and temperature (cf. Fig. S1 Supplementary information), the measured lifetime can be converted into a temperature profile. The spatial resolution of the temperature and concentration measurement is $1\ \mu\text{m}$ and $0.25\ \mu\text{m}$, respectively. The concentration ratio for the Soret coefficient was determined from the fluorescence intensity ratio. After reaching the equilibrium of the concentration profile, the concentration ratio $c(x, y)$ was evaluated as follows,

$$\frac{c(x, y)}{c(x_{\text{ref}}, y)} = \frac{I(x, y)}{I(x_{\text{ref}}, y)} \quad (2)$$

with the intensity $I(x, y)$. y_{ref} is the center of the measuring channel.

2.5. Data evaluation

In a diluted solution ($c \ll 1$), the flux equation in Eq.1 in the steady state was expressed as,

$$\nabla c = -c S_T \nabla T, \quad (3)$$

with the temperature T and the Soret coefficient S_T . In the measuring channel, one-dimensional temperature gradient happened along a transverse direction of the measuring channel. For this reason, the averaged temperature $\bar{T}(x)$

and concentration ratio $\bar{c}(x)/\bar{c}(x_{\text{ref}})$ along the longitudinal direction of the measuring channel were used for the Soret coefficient. The size of the field of view is $256 \mu\text{m}$ (x) by $256 \mu\text{m}$ (y). The number of pixels for temperature measurement is 256 by 256, so that each pixel is $1 \mu\text{m} \times 1 \mu\text{m}$. The number of pixels for intensity measurements is 1024 by 892 where the length of each pixel is $0.25 \mu\text{m}$ (Δx) by $0.29 \mu\text{m}$ (Δy). The average temperature is calculated from 256 pixels along y -axis in the field of view. The average intensity is calculated by 892 pixels along y -axis. Based on averaged values, we rearranged Eq.3 using $\nabla c = dc/dx$ and $\nabla T = dT/dx$ as follows:

$$\ln \frac{\bar{c}(x)}{\bar{c}(x_{\text{ref}})} = \ln \frac{\bar{I}(x)}{\bar{I}(x_{\text{ref}})} = S_T(\bar{T}(x_{\text{ref}})) - \bar{T}(x) \quad (4)$$

According to eq.4, the logarithmic concentration ratio depends linearly on the temperature difference $T(x_{\text{ref},y,z}) - T(x, y, z)$. The logarithmic concentration ratio was determined from the logarithmic fluorescence intensity ratio. The slope in the linear relation is the Soret coefficient. The reference location in this study was at the center of the measuring channel.

2.6. Uncertainty analysis

The uncertainty of the Soret coefficient was calculated from the uncertainty of the logarithmic concentration ratio and the temperature. The averaged uncertainty of the intensity ratio was 3.4%. That of the temperature was $\delta T = 0.28 \text{ K}$. Then, we calculated the uncertainty of the slope, which is identical with the Soret coefficient. We included the deviations of temperature and logarithmic intensity ratio following the York method [41] implemented in the commercial plot software ORIGIN [42]. This resulted in an averaged uncertainty of the Soret coefficient of 9% based on the 95% confidence level [43].

3. Results

3.1. Temperature profile in the thermophoretic microfluidic cells

In the thermophoretic microfluidic cell, the precise characterization and stability of the temperature profile are crucial since this profile results in the concentration distribution in the measuring channel. Figure 3(a) presents the temperature distribution measured by FLIM without and with a temperature gradient. In the absence of a temperature gradient, we find a homogeneous temperature distribution. Increasing the temperature in the heating channel (left) to 40°C and decreasing the temperature in the cooling channel (right) to 10°C leads to a gradual temperature decrease along the x -axis. The measured temperature in Fig. 3(a) was independent of the y -direction, so that we achieved an one-dimensional temperature profile in the measuring channel as intended.

Fig. 3(b) shows the y -axis averaged temperature profile across the channel. Without the temperature gradient, the mean temperature is 21.4°C , while with the temperature gradient, the mean temperature at the center of the measuring

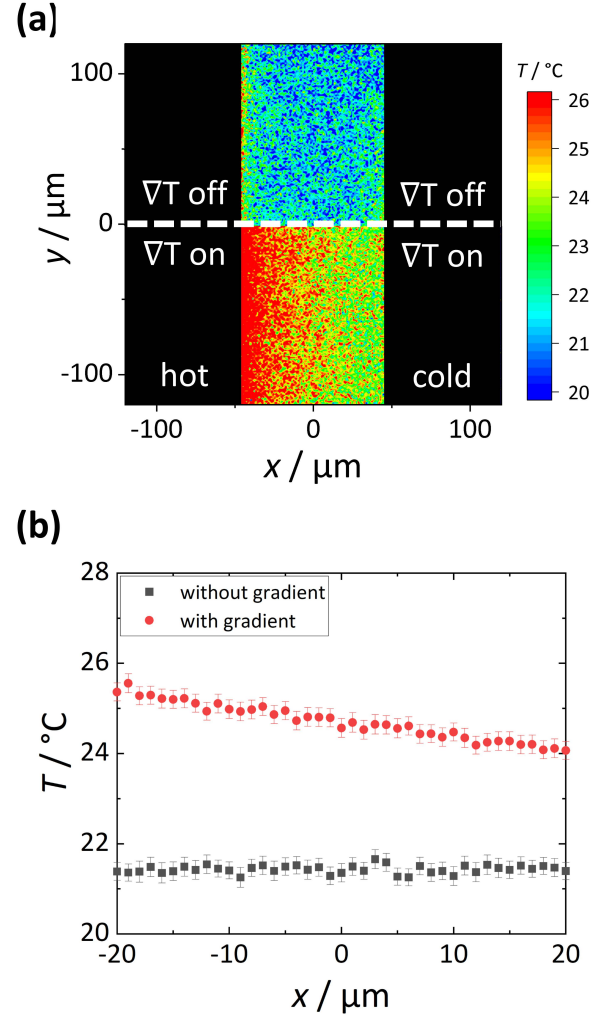


Figure 3: Temperature distribution measured by fluorescence lifetime imaging microscopy (FLIM) without temperature gradient (upper figure, $T_{\text{mean}} = 21.4^\circ\text{C}$) and $\nabla T = 34207 \text{ K/m}$ (bottom figure, $T_{\text{mean}} = 24.7^\circ\text{C}$). (b) Graph of the line-averaged temperature along the y -axis as function of x . The resolution of the temperature profile is $1 \mu\text{m}$

channel is 24.7°C and a gradient of around $33000 \pm 1000 \text{ K/m}$ establishes inside the measuring channel. Note, that the achieved temperature gradient depends not only on the temperatures of the thermostats, but also on the surrounding temperature. Typically observed gradients lie between of 32000 and 34000 K/m. Considering the temperatures in the heating and cooling channel of 10°C and 40°C , we would expect ideally an almost three-times larger temperature gradient of roughly 92000 K/m. The reason for the low temperature gradient is a large temperature drop within the PMMA-wall with a low thermal conductivity with $k = 0.19 \text{ W/mK}$ [44] separating the measuring channel from the heating and cooling channel. This implies that the temperature gradient in the measuring channel can be increased by using a wall material with a high thermal conductivity.

In order to characterize the temperature profile for different mean temperatures, we varied the cooling and heating

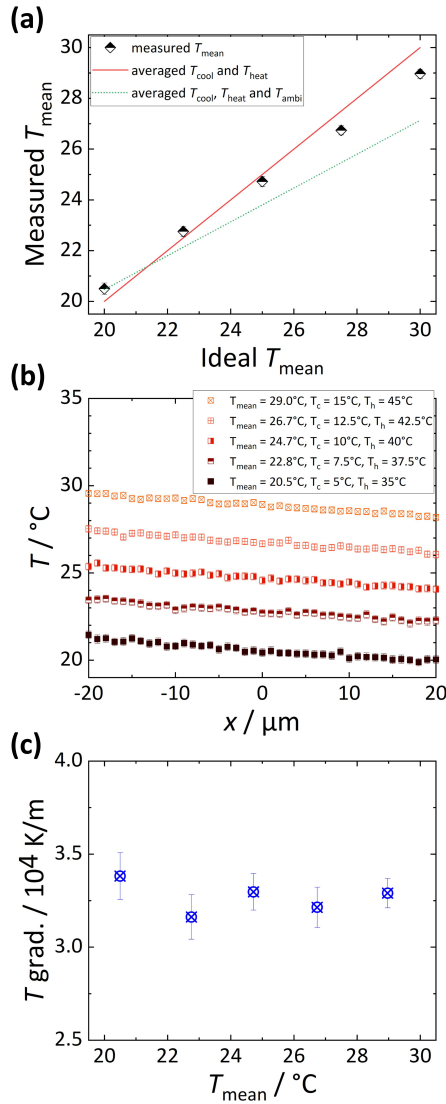


Figure 4: (a) Comparison of measured and calculated mean temperatures in the measuring channel. The solid red line represents the ideal mean temperature $T_{\text{calch}} = 0.5(T_{\text{cool}} + T_{\text{heat}})$ calculated from the temperatures of the heating and cooling water at T_{heat} and T_{cool} , respectively. The dotted green line corresponds to $T_{\text{calcha}} = (1/3)(T_{\text{cool}} + T_{\text{heat}} + T_{\text{ambi}})$ taking the ambient temperature T_{ambi} in the lab into account. (b) Change of the y-axis averaged temperature across the measurement channel for different temperatures in the thermostating channels. Note that only the temperature profile in the center of the measuring channel is shown. (c) Temperature gradient as a function of the mean temperature.

temperature between 5–15°C and 35–45°C, respectively. The solid red line in Fig. 4(a) presents the calculated average $T_{\text{calch}} = 0.5(T_{\text{cool}} + T_{\text{heat}})$ in comparison with the measured mean temperature T_{mean} at the center of the measuring channel (diamonds). The mean temperature T_{mean} is the averaged temperature of the y-axis line-averaged temperature as a function of x-axis within $\pm 1 \mu\text{m}$. In Fig. 4(a), it is shown that the slope of the measured mean temperature is lower than the expected mean temperature (red line). This is caused

by a heat exchange between the cell and the surrounding environment at ambient temperature leading to higher temperatures at low and lower temperatures at higher temperatures. The influence of the ambient temperature might be estimated by taking the average of all three temperatures $T_{\text{calcha}} = (1/3)(T_{\text{cool}} + T_{\text{heat}} + T_{\text{ambi}})$ indicated by the dotted green line in Fig. 4(a). It turns out that the actual measured temperatures lie between the two calculated lines. These observations emphasize that it is necessary to measure the temperature profile within the measuring channel as temperature changes in the environment will have an impact on the profile in the microfluidic cell.

We performed measurements at different mean temperatures by keeping the temperature difference between the heating and cooling channel the same and by varying the temperatures in steps of 2.5°C over a temperature range of 10°C. Figure 4(b) shows the y-axis averaged temperature profiles for different mean temperatures across the channel in the x-direction. In all cases, we observe a one-dimensional temperature profile independent of the mean temperature and similar temperature gradients. The gradients vary from 32000 K/m ($T_{\text{cool}} = 7.5^\circ\text{C}$, $T_{\text{heat}} = 37.5^\circ\text{C}$) to 34000 K/m ($T_{\text{cool}} = 5^\circ\text{C}$, $T_{\text{heat}} = 35^\circ\text{C}$). As can be seen in Fig. 4(c), the measured temperature gradient does not show a systematic trend with the mean temperature. The fluctuations of the temperature gradient are of the order of 10%.

Additionally, we characterized the temperature profile in y-direction and at different heights z inside the measuring channel to ensure a one-dimensional profile. Figure 5(a) shows the temperature profile at three different y-positions as function of x , whereas the temperatures of the thermostats were set to 10°C and 40°C. We observe that the temperature profiles differ up to about 1°C for the three different y-positions. Many factors may be responsible for this discrepancy, such as the heat exchange with the surrounding, fabrication tolerances of the cell and other geometrical differences such as flow connectors and the thermal contact with microscope. If we assume that the heat exchange between the measuring channel and the thermostated channels is the main reason, we expect a monotonous change of the temperature in y-direction gradually decreasing from 3 mm to -3 mm due to the cross flow configuration of the cooling and heating fluid as indicated in the inset of Fig. 5. However, since there is no systematic temperature variation, the heat exchange with the thermostated channels is not the only reason for this discrepancy. Although the influence of geometric factors cannot be quantified, from Fig. 4(a), we infer that the ambient temperature couples into the small microfluidic chip, but also manufacturing tolerances of the wall between measuring and thermostated channels will influence the observed temperature profile. As shown in Fig. 5(b), temperatures along the z -axis are also slightly different, even though the geometrical changes along the z -axis has a smaller variation than along the y -axis. From these results in Fig. 5(a) and (b), we conclude that the temperature differences along the channel are also caused by geometrical factors. However, the temperature gradient along the y -axis

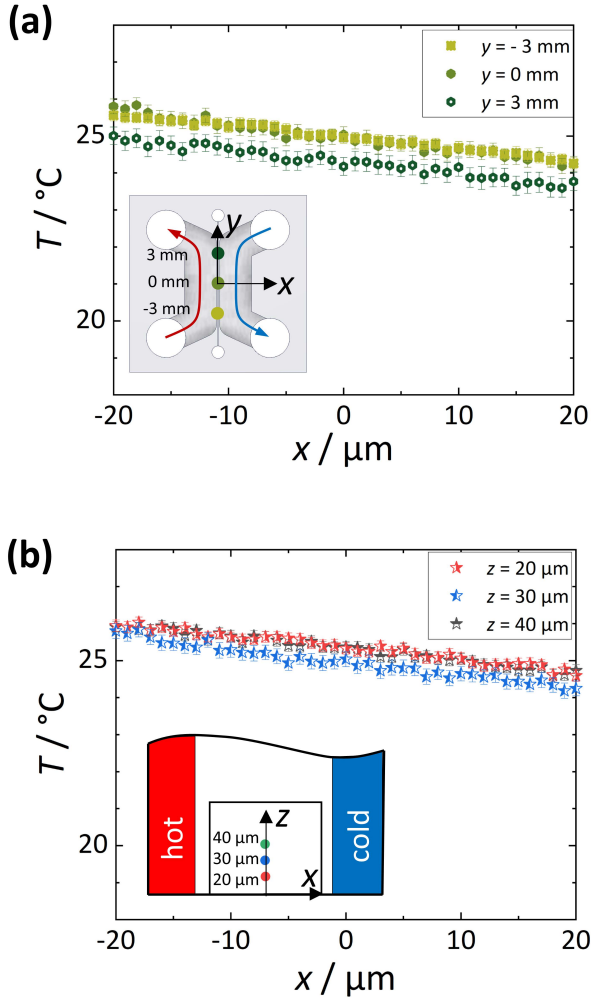


Figure 5: Graphs of the y -axis averaged temperature as a function of x at (a) three different locations along the measuring channel ($y = -3, 0, 3$ mm). The inset illustrates the measuring positions. (b) The y -axis Line-averaged temperature at three different heights ($z = 20, 30, 40$ μm). Inset shows the locations.

is with 333 K/m only 1% of the temperature gradient along the x -axis, so that we can neglect it. In the following, we consider a one-dimensional temperature gradient along the x -axis for the calculation of the Soret coefficient.

3.2. Intensity ratio profile in the thermophoretic microfluidic cells

Figure 6(a) shows an image of the intensity ratio $\bar{I}/\bar{I}_{x=0}$ distribution within the measuring channel. According to Eq. 2, the intensity ratio is identical to the concentration ratio $\bar{c}/\bar{c}_{x=0}$, which is required to calculate the Soret coefficient in Eq. 4. The upper and bottom parts of Fig. 6(a) have been taken at a mean temperature of $T_{\text{mean}} = 24.7^{\circ}\text{C}$ without and with a temperature gradient of $\nabla T = 33000$ K/m, respectively. In the absence of a temperature gradient, the intensity ratio is constant in the center of the channel, indicating a homogeneous distribution of particles. Towards the walls, we observe a drop of the intensity, which could be caused by

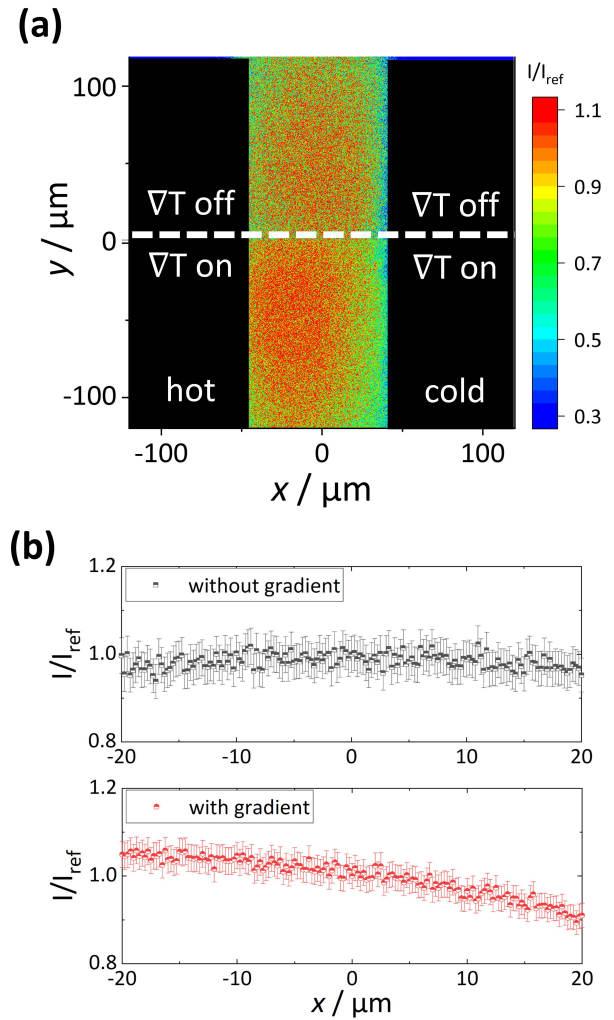


Figure 6: Image of the intensity ratio distribution measured by fluorescence intensity without temperature gradient (upper figure, $T_{\text{mean}} = 21.4^{\circ}\text{C}$) and $\nabla T = 33000$ K/m (bottom figure, $T_{\text{mean}} = 24.7^{\circ}\text{C}$). (b) Graph of y -axis averaged intensity ratio as a function of x without (top) and with (bottom) temperature gradient, respectively.

reflections at the wall or interfacial effects close to the wall. Therefore, in the following, we restrict our analysis to the center of the cell.

To quantify the intensity ratio profile, the y -axis averaged intensity ratio is used. As shown in the upper part of Fig. 6(b), the intensity ratio is constant without an applied temperature gradient while we observe an asymmetric distribution, if a temperature gradient is applied (cf. bottom part of Fig. 6(b)). The intensity ratio is not linearly varying across the channel, but shows an exponential profile as expected according to Eq. 4.

Before calculating the Soret coefficient, we also need to check the dependence of the concentration ratio on the y - and z -axes in a similar way as for the temperature profile. Figure 7(a) shows the averaged intensity ratio as a function of x along the y -direction. We observe that the intensity ratio is almost identical at the three locations. This is in contrast

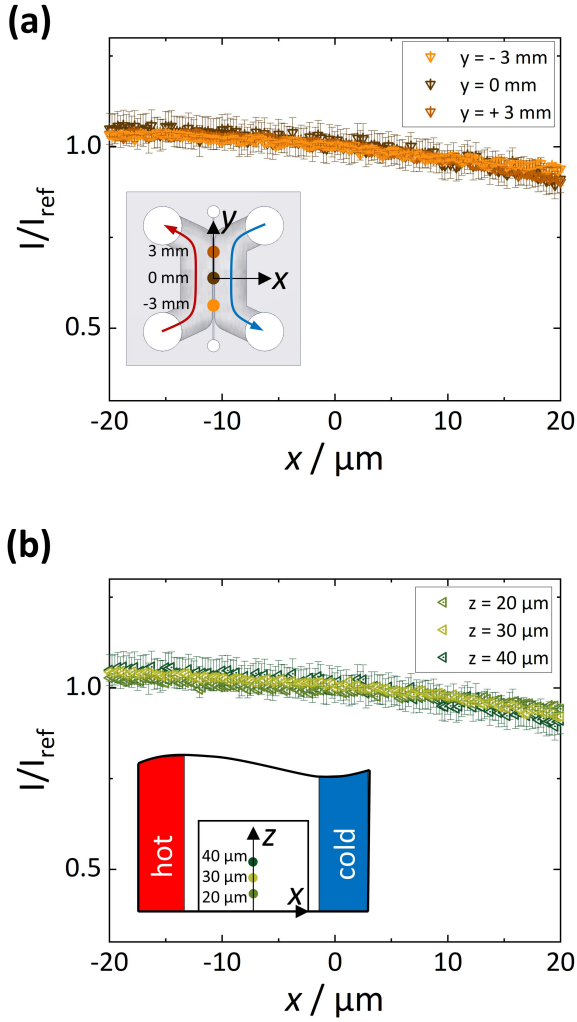


Figure 7: Graphs of the line-averaged intensity ratio along the y -axis as function of x at (a) three different locations ($y = -3, 0, 3$ mm) and (b) three different heights ($z = 20, 30, 40$ μm).

to the slight variation of the temperature profile along the y -direction. We assume that although the geometrical differences leading to a temperature difference along the measuring channel, the averaged variation of temperature is within 0.4 K resulting in an intensity ratio modulation of 0.04, if we assume a Soret coefficient of 0.1 K^{-1} . This implies that the variation of the intensity ratio along the y -axis is negligible. Fig. 7(b) shows that the intensity ratio at different heights also overlaps. Therefore, we can conclude that we have one-dimensional temperature and the concentration ratio profiles in the measuring channel which can be used to calculate the Soret coefficient accordingly.

In addition, we investigated the effect of free convection on the concentration profile in the measuring channel, which would distort the concentration profile. Based on a one-dimensional temperature profile in the measuring channel, we can simulate the temperature and concentration profile. In the simulation, we observe free convection in the measuring channel, whereas the magnitude of free convection

velocity is comparable with the thermophoretic velocity (cf. Fig. S2 in the Supplementary Information). Nevertheless, the obtained concentration profiles are almost the same with and without free convection (cf. Fig. S3 in the Supplementary Information). Additionally, the slopes of the logarithmic concentration ratios as function of x and $T - T_{\text{ref}}$ along the z -axis overlap, so that we can ignore free convection for the analysis of S_T . Furthermore, we investigate whether measurements of thermophobic particles ($S_T > 0$) are possible. The simulated results of thermophobic particles reveal that the effect on the concentration profile is weak (cf. Fig. S5 in the Supplementary Information). It means that the cell can be used to evaluate S_T of thermophobic particles using Eq. 4. Note that, since the natural convection velocity in the channel is confined by the shortest length of the channel, a smaller channel ensures reliable concentration profiles to determine Soret coefficients. A detailed description of the simulation of free convection and thermophoresis is presented in the Supplementary Information.

3.3. Evaluation of the Soret coefficient

The measured temperature and intensity ratio in the measuring channel were used to calculate the Soret coefficient according to Eq. 4. Figure 8(a) shows the natural logarithm of the measured intensity ratio as function of the temperature difference. During the experiments, we set the cooling and heating fluid temperatures to 10°C and 40°C , respectively. The solid lines are linear fits of the logarithmic intensity ratio as function of the temperature difference. Note, that the linearly fitted lines of run 1 and 2 overlap. The corresponding slopes are $-0.114 \pm 0.009 \text{ K}^{-1}$ and $-0.110 \pm 0.010 \text{ K}^{-1}$, respectively. The uncertainties include the errors of temperature differences and concentration ratios.

Figure 8(b) shows the temperature dependence of the Soret coefficient measured in the microfluidic channel cell. In order to verify the cell, we compared the obtained S_T values with the data measured with the TDFRS set-up, which has been validated in the Fontainebleau benchmark using three binary organic mixtures [45]. Note that, it is impossible to certify the microfluidic cell using the same mixtures, [45] because, with a confocal microscope, we cannot measure concentration changes of organic solvents. The data points shown in Fig. 8(b) and their error bars are additionally listed in Table 1. The fitted curve is described by the empirical equation [46],

$$S_T = S_T^\infty \left[1 - \exp\left(\frac{T^* - T}{\tilde{T}}\right) \right], \quad (5)$$

where S_T^∞ , T^* and \tilde{T} are empirical parameters that refer to the Soret coefficient at infinite temperature, the temperature at which a sign change of S_T occurs, and a parameter to describe the curvature, respectively. The empirical parameters S_T^∞ , T^* and \tilde{T} determined for the TDFRS data are $0.20 \pm 0.03 \text{ K}^{-1}$, $323.4 \pm 0.89 \text{ K}$ and $61.6 \pm 6.32 \text{ K}$, respectively. It turns out that the averaged deviation of Soret coefficients measured with the microfluidic cell is 7.8% from the fitted

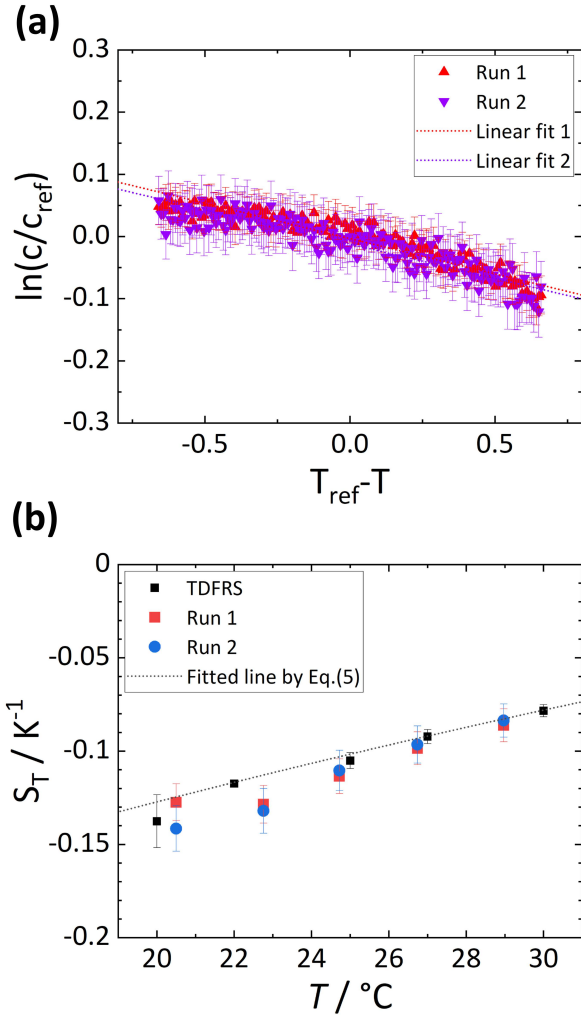


Figure 8: (a) Logarithmic intensity ratio as a function of temperature difference for run 1 and 2. ($T_{cool} = 10^\circ C$, $T_{heat} = 40^\circ C$, $T_{mean} = 24.7^\circ C$) The red and blue dotted lines refer to a linear fit of the data of run 1 and run 2, respectively. (b) Comparison of the Soret coefficients of unwashed polystyrene particles ($d = 25$ nm, 1%) measured in run 1 (red square), run 2 (blue bullet) and with TDFRS (black square) connected with a dotted line). The dotted line corresponds to a fit of the TDFRS data using Eq. 5.

curve according to Eq. 5 in the investigated temperature range.

Another advantage of the instrument is that we can control the mean temperature between 20–30°C to perform temperature dependent measurements of the Soret coefficient. The obtained Soret coefficients of the G25-particles increase between 20°C and 30°C from -0.138 K^{-1} to -0.078 K^{-1} . A similar weak temperature dependence has been observed before another batch of the same particles [38] and is typical for solutes in water at high dilution and can be described in Eq. 5 [46]. This empirical equation reflects that the thermophoretic behavior of aqueous systems is dominated by hydrogen bonds. With increasing temperature the strength of the hydrogen bonds is weakened leading to an

Table 1

Soret coefficients of G25-particles (1% wt) measured in the microfluidic channel cell in comparison with TDFRS results. The uncertainties include the errors of temperature differences and concentration ratios.

$T / ^\circ C$	S_T / K^{-1} Run 1	S_T / K^{-1} Run 2	$T / ^\circ C$	S_T / K^{-1} TDFRS
20.5	-0.127 ± 0.010	-0.142 ± 0.012	20	-0.138 ± 0.014
22.8	-0.129 ± 0.010	-0.132 ± 0.012	22	-0.117 ± 0.001
24.7	-0.114 ± 0.009	-0.110 ± 0.011	25	-0.105 ± 0.004
26.7	-0.099 ± 0.009	-0.097 ± 0.010	27	-0.092 ± 0.004
29.0	-0.086 ± 0.009	-0.084 ± 0.009	30	-0.078 ± 0.003

increase of S_T and a decrease of the temperature dependent slope [6]. The latter cannot be observed for the G25 particles in the investigated temperature range, since the temperature dependent slope of S_T remains almost constant.

As mentioned before, the surrounding temperature influences the temperature profile within the measuring channel, therefore an expansion of the temperature range will require a thermostated housing of the set-up to reach a good temperature stability. In conclusion, the proposed thermophoretic microfluidic cell provides reliable and reproducible temperature dependent measurements of S_T .

4. Conclusion

In summary, we propose a thermophoretic microfluidic cell for quantitative measurements of the Soret coefficient of colloidal particles or proteins. In the developed microfluidic cell the actual measuring channel is located between heating and cooling channel to establish a temperature gradient across the measuring channel. As a test system, we used fluorescently labeled polystyrene particles with a diameter of 25 nm. FLIM with RhB is utilized for probing the spatial temperature profile inside the measuring channel. The established concentration ratio in the steady state is determined from the fluorescence intensity ratio. The characterization of the thermophoretic cell reveals that a one-dimensional temperature profile is achieved. The established concentration ratio profile, which is equal to the measurable intensity ratio profile, is used to determine the Soret coefficient. In the entire investigated temperature range, the obtained S_T -values of the colloidal particles deviate on averaged by 7.8% from the fitted curve describing the TDFRS results. We demonstrated further that the device is suitable to perform temperature dependent measurements. So far, we varied the mean temperature between 20°C and 30°C. An expansion of the temperature range will be possible, if a thermostated housing is used to reach a good temperature stability. As mentioned, characterization measurements revealed that the ambient surrounding temperature influences the temperature profile inside the measuring channel. This effect raises as the temperature difference between the measuring channel and the environment increases. In conclusion, the proposed thermophoretic microfluidic cell provides reliable and reproducible temperature dependent measurements of S_T for

large colloids ($> 1 \mu\text{m}$) and smaller fluorescently labelled particles or (bio-)macromolecules.

The proposed cell has several advantages compared to conventional methods, which are often limited to binary mixtures. The presented thermophoretic microfluidic device allows the study of specific fluorescently labeled or large solute macromolecules in multi-component mixtures such as buffer solutions. For instance, it will be possible to study the thermophoretic behavior of solutes for buffer solutions of different ionic strength or pH. The thermophoretic microfluidic cell has also a fairly short equilibration time $\tau = w_m^2/(\pi^2 D)$, which depends on the measuring channel width w_m and the mass diffusion coefficient D [47]. Even for larger colloidal particles with a diameter of $1 \mu\text{m}$, we find equilibration times of roughly 1 hour, which should be accessible if evaporation of the solvent and photobleaching of the dye are prevented. Note that, the sedimentation velocity of $1 \mu\text{m}$ PS particle is 35.2 nm/s [48]. The channel height is $76 \mu\text{m}$, which leads to the retention time of sedimentation of 1.5 hours. Therefore, sedimentation will influence the thermophoretic motion so that a mixture of water and heavy water (D_2O) should be used to match the density of the solvent with that of the particles. Another advantage of this cell is the small channel volume lower than $20 \mu\text{L}$ including connectors which makes it suitable for the study of rare biological compounds. With this cell, it will also be possible to investigate the thermophoretic movement in nematic phases or a crowded environment. The latter is especially interesting to study transport in biomimetic systems. This device will help to extend our fundamental understanding of thermophoresis in complex environments and might also be suitable to develop new analytical methods to characterize and separate colloidal synthetic and natural particles.

Acknowledgments

We thank the JCNS workshop and ZEA 1 for their advice and fabrication of the cells. We are grateful to Jan Dhont for inspiring ideas and his generous support of our work. NL acknowledges the support by the Humboldt foundation and SM acknowledges the support by the International Helmholtz Research School of Biophysics and Soft Matter (BioSoft).

References

- [1] S. R. de Groot. *Thermodynamics of irreversible processes*. North Holland, Amsterdam, 1966.
- [2] W. Köhler and K. I. Morozov. The sorot effect in liquid mixtures - a review. *J. Non-Equil. Thermodyn.*, 41:151–197, 2016.
- [3] P. Baaske, F. M. Weinert, S. Duhr, K. H. Lemke, M. J. Russell, and D. Braun. Extreme accumulation of nucleotides in simulated hydrothermal pore systems. *Proc. Natl. Acad. Sci. USA*, 104:9346–9351, 2007.
- [4] Doreen Niether, Dmity Afanasenkau, Jan K. G. Dhont, and Simone Wiegand. Accumulation of formamide in hydrothermal pores to form prebiotic nucleobases. *Proc. Natl. Acad. Sci. USA*, 113:4272–4277, 2016.
- [5] Mufarreh Asmari, Ratih Ratih, Hassan A. Alhazmi, and Sami El Deeb. Thermophoresis for characterizing biomolecular interaction. *Methods*, 146:107–119, 2018.
- [6] D. Niether and S. Wiegand. Thermophoresis of biological and biocompatible compounds in aqueous solution. *J. Phys. Condens. Matter*, 31(50):503003, 2019.
- [7] Fei Tian, Ziwei Han, Jinqi Deng, Chao Liu, and Jiashu Sun. Thermomicrofluidics for biosensing applications. *VIEW*, page 20200148, 2021.
- [8] Thomas J. Salez, Bo Tao Huang, Maud Rietjens, Marco Bonetti, Cécile Wiertel-Gasquet, Michel Roger, Cleber Lopes Filomeno, Emmanuelle Dubois, Régine Perzynski, and Sawako Nakamae. Can charged colloidal particles increase the thermoelectric energy conversion efficiency? *Phys. Chem. Chem. Phys.*, 19:9409–9416, 2017.
- [9] Cheng-Gong Han, Xin Qian, Qikai Li, Biao Deng, Yongbin Zhu, Zhijia Han, Wenqing Zhang, Weichao Wang, Shien-Ping Feng, Gang Chen, and Weishu Liu. Giant thermopower of ionic gelatin near room temperature. *Science*, 368(6495):1091–1098, 2020.
- [10] Yanhua Jia, Qinglin Jiang, Hengda Sun, Peipei Liu, Dehua Hu, Yanzhong Pei, Weishu Liu, Xavier Crispin, Simone Fabiano, Yuguang Ma, and Yong Cao. Wearable thermoelectric materials and devices for self-powered electronic systems. *Adv. Mater.*, 33:e2102990, 2021.
- [11] Philip Ball and John E. Hallsworth. Water structure and chaotropy: their uses, abuses and biological implications. *Phys. Chem. Chem. Phys.*, 17:8297–8305, 2015.
- [12] S. R. de Groot and P. Mazur. *Non-equilibrium Thermodynamics*. Dover, New York, 1984.
- [13] A. Parola and R. Piazza. Particle thermophoresis in liquids. *Eur. Phys. J. E*, 15:255–263, 2004.
- [14] P. A. Artola, B. Rousseau, and G. Galliero. A new model for thermal diffusion: Kinetic approach. *J. Am. Chem. Soc.*, 130:10963–10969, 2008.
- [15] A. Würger. Thermal non-equilibrium transport in colloids. *Rep. Prog. Phys.*, 73:126601, 2010.
- [16] S. Di Lecce, T. Albrecht, and F. Bresme. The role of ion-water interactions in determining the sorot coefficient of licl aqueous solutions. *Phys. Chem. Chem. Phys.*, 19:9575–9583, 2017.
- [17] R. Rusconi, L. Isa, and R. Piazza. Thermal-lensing measurement of particle thermophoresis in aqueous dispersions. *J. Opt. Soc. Am. B*, 21:605–616, 2004.
- [18] P. Polyakov and S. Wiegand. Investigation of the sorot effect in aqueous and non-aqueous mixtures by the thermal lens technique. *Phys. Chem. Chem. Phys.*, 11:864–871, 2009.
- [19] W. Köhler and P. Rossmanith. Aspects of thermal-diffusion forced rayleigh-scattering - heterodyne-detection, active phase tracking, and experimental constraints. *J. Phys. Chem.*, 99:5838–5847, 1995.
- [20] S. Wiegand, H. Ning, and H. Krieger. Thermal diffusion forced rayleigh scattering setup optimized for aqueous mixtures. *J. Phys. Chem. B*, 111(51):14169–14174, 2007.
- [21] R. Piazza. Thermal diffusion in ionic micellar solutions. *Philos. Mag.*, 83:2067–2085, 2003.
- [22] A. Köninger, B. Meier, and W. Köhler. Measurement of the sorot, diffusion, and thermal diffusion coefficients of three binary organic benchmark mixtures and of ethanol-water mixtures using a beam deflection technique. *Philos. Mag.*, 89:907–923, 2009.
- [23] I. Dueramae, M. Yoneyama, N. Shinyashiki, S. Yagihara, and R. Kita. Thermal diffusion of aqueous solution of acetylated dextran: The effect of hydrophobicity using optical beam deflection technique. *Int. J. Heat Mass Transf.*, 132:997–1003, 2019.
- [24] M. M. Bou-Ali, O. Ecenarro, J. A. Madariaga, C. M. Santamaria, and J. J. Valencia. Thermogravitational measurement of the sorot coefficient of liquid mixtures. *J. Phys.: Condens. Matter*, 10(15):3321–3331, 1998.
- [25] M. Gebhardt and W. Köhler. What can be learned from optical two-color diffusion and thermodiffusion experiments on ternary fluid mixtures? *J. Chem. Phys.*, 142:084506, 2015.
- [26] P. Blanco, M. M. Bou-Ali, J. K. Platten, D. A. de Mezquia, J. A. Madariaga, and C. Santamaria. Thermodiffusion coefficients of binary and ternary hydrocarbon mixtures. *J. Chem. Phys.*, 132(11):114506, 2010.

- [27] D. Vigolo, R. Rusconi, H. A. Stone, and R. Piazza. Thermophoresis: microfluidics characterization and separation. *Soft Matter*, 6(15):3489–3493, 2010.
- [28] Susanne A. I. Seidel, Patricia M. Dijkman, Wendy A. Lea, Geert van den Bogaart, Moran Jerabek-Willemsen, Ana Lazic, Jeremiah S. Joseph, Prakash Srinivasan, Philipp Baaske, Anton Simeonov, Ilia Katritch, Fernando A. Melo, John E. Ladbury, Gideon Schreiber, Anthony Watts, Dieter Braun, and Stefan Duhr. Microscale thermophoresis quantifies biomolecular interactions under previously challenging conditions. *Methods*, 59(3):301–315, 2013.
- [29] Yi Zhou, Chun Yang, Yee Cheong Lam, and Xiaoyang Huang. Thermophoresis of charged colloidal particles in aqueous media – effect of particle size. *Int. J. Heat Mass Transf.*, 101:1283–1291, 2016.
- [30] Tetsuro Tsuji, Kosuke Kozai, Hideto Ishino, and Satoyuki Kawano. Direct observations of thermophoresis in microfluidic systems. *Micro Nano Lett.*, 12(8):520–525, 2017.
- [31] Daniel Lauster, Simon Klenk, Kai Ludwig, Saba Nojoudi, Sandra Behren, Lutz Adam, Marlina Stadtmüller, Sandra Saenger, Stephanie Zimmer, Katja Hönzke, Ling Yao, Ute Hoffmann, Markus Bardua, Alf Hamann, Martin Witzernath, Leif E. Sander, Thorsten Wolff, Andreas C. Hocke, Stefan Hippenstiel, Sacha de Carlo, Jens Neudecker, Klaus Osterrieder, Nediljko Budisa, Roland R. Netz, Christoph Böttcher, Susanne Liese, Andreas Herrmann, and Christian P. R. Hackenberger. Phage capsid nanoparticles with defined ligand arrangement block influenza virus entry. *Nat. Nanotechnol.*, 15(5):373–379, 2020.
- [32] Alexandra C. Walls, M. Alejandra Tortorici, Berend-Jan Bosch, Brandon Frenz, Peter J. M. Rottier, Frank DiMaio, Félix A. Rey, and David Veelsler. Cryo-electron microscopy structure of a coronavirus spike glycoprotein trimer. *Nature*, 531(7592):114–117, 2016.
- [33] Arne Ittner, Sook Wern Chua, Josefine Bertz, Alexander Volkerling, Julia van der Hoven, Amadeus Gladbach, Magdalena Przybyla, Mian Bi, Annika van Hummel, Claire H. Stevens, Stefania Ippati, Lisa S. Suh, Alexander Macmillan, Greg Sutherland, Jillian J. Kril, Ana P. G. Silva, Joel P. Mackay, Anne Poljak, Fabien Delerue, Yazid D. Ke, and Lars M. Ittner. Site-specific phosphorylation of tau inhibits amyloid- β toxicity in alzheimer’s mice. *Science*, 354(6314):904–908, 2016.
- [34] Ruoyu Dong, Yi Zhou, Chun Yang, and Bing-Yang Cao. Experimental study on thermophoresis of colloids in aqueous surfactant solutions. *J. Phys.: Condens. Matter*, 27(49):495102, 2015.
- [35] Namkyu Lee and Simone Wiegand. Thermophoretic micron-scale devices: Practical approach and review. *Entropy*, 22(9):950, 2020.
- [36] Y. Cengel. *Heat and mass transfer: fundamentals and applications*. McGraw-Hill Higher Education, 2014.
- [37] M. Annoni, L. Rebaioli, and Q. Semeraro. Thin wall geometrical quality improvement in micromilling. *Int. J. Adv. Manuf.*, 79(5-8):881–895, 2015.
- [38] Olga Syshchyk, Dzmitry Afanasenkau, Zilin Wang, Hartmut Kriegs, Johan Buitenhuis, and Simone Wiegand. Influence of temperature and charge effects on thermophoresis of polystyrene beads. *Eur. Phys. J. E*, 39(12):129, 2016.
- [39] A. Becker, W. Köhler, and B. Müller. A scanning michelson interferometer for the measurement of the concentration and temperature derivative of the refractive- index of liquids. *Ber. Bunsen-Ges. Phys. Chem. Chem. Phys.*, 99(4):600–608, 1995.
- [40] C. B. Müller, K. Weiss, A. Loman, J. Enderlein, and W. Richtering. Remote temperature measurements in femto-liter volumes using dual-focus-fluorescence correlation spectroscopy. *Lab Chip*, 9(9):1248–1253, 2009.
- [41] D. York, N. M. Evensen, M. L. Martínez, and J. de Basabe Delgado. Unified equations for the slope, intercept, and standard errors of the best straight line. *Am. J. Phys.*, 72(3):367–375, 2004.
- [42] OriginPro 2019. Originlab corporation. (Northampton, MA, USA).
- [43] Robert J. Moffat. Describing the uncertainties in experimental results. *Exp. Therm. Fluid Sci.*, 1(1):3–17, 1988.
- [44] M. J. Assael, S. Botsios, K. Gialou, and I. N. Metaxa. Thermal conductivity of polymethyl methacrylate (pmma) and borosilicate crown glass bk7. *Int. J. Thermophys.*, 26(5):1595–1605, 2005.
- [45] J. K. Platten, M. M. Bou-Ali, P. Costesque, J. F. Dutrieux, W. Köhler, C. Leppla, S. Wiegand, and G. Wittko. Benchmark values for the solet, thermal diffusion and diffusion coefficients of three binary organic liquid mixtures. *Philos. Mag.*, 83:1965–1971, 2003.
- [46] S. Iacopini, R. Rusconi, and R. Piazza. The macromolecular tourist: Universal temperature dependence of thermal diffusion in aqueous colloidal suspensions. *Eur. Phys. J. E*, 19:59–67, 2006.
- [47] S. Wiegand. Thermal diffusion in liquid mixtures and polymer solutions. *J. Phys.: Condens. Matter*, 16(10):R357–R379, 2004.
- [48] M. Braibanti, D. Vigolo, and R. Piazza. Does thermophoretic mobility depend on particle size? *Phys. Rev. Lett.*, 100(10):108303–1–108303–4, 2008.